Time-resolved study of ultrafast dephasing processes in solution

A. Kummrow, A. Lau, and K. Lenz
Max-Born-Institut für Nichtlineare Optik und Kurzzeitspektroskopie, Rudower Chaussee 6, D-12474 Berlin, Germany
(Received 26 December 1995; revised manuscript received 7 October 1996)

Electronic dephasing of solutions of *all-trans*-bis-(dimethylamino)-heptamethinium chloride, its photoisomer, and of 1,1′,3,3,3′,3′-hexamethylindotricarbocyanine iodide (HITCI) is studied using forced light scattering by broad-bandwidth incoherent pump lasers in the wavelength region from 440 to 770 nm. The dephasing slows down as the pump laser wavelength is tuned over the 0-0 transition. Photoisomer and parent heptamethine molecule show comparable behavior in dephasing experiments. Absorption line-shape analysis including resonance Raman experiments indicates a considerable spectral cross relaxation in the absorption band of the parent molecule. The results for HITCI are close to those reported for two-pulse femtosecond photon echoes. [S1050-2947(97)06202-1]

PACS number(s): 42.50.Md, 42.65.Re, 78.47.+p

I. INTRODUCTION

Monitoring optical dephasing processes is an important probe of static and dynamic properties of condensed matter, and has provided substantial information on the dynamics of elementary excitations in liquids. Solvation dynamics following electronic rearrangement of solute molecules, e.g., dye molecules or reactive species, has a dominant influence on the energetic position and shape of the potential energy surface. With respect to chemical reactions in liquids, the relaxation of the solvent molecules modifies the effective potential energy surface dynamically and might even prevent back reaction of the evolving products [1].

The linear response of the solvent can be described by the autocorrelation function $M(t)$ of the fluctuations in the electronic transition energy of the solute molecules [2,3]. Molecular dynamics simulations (assuming Lennard-Jones liquids plus Coulomb potentials) were carried out for a number of simple solvents to determine $M(t)$ [2–4]. Direct experimental access to $M(t)$ is possible observing the time-dependent Stokes shift of the fluorescence, but the initial ultrafast dynamics on a time scale of a few 10 fs was not resolved up to now by this technique, mainly because of the difficulty of obtaining sufficient time resolution [1,2]. In addition, finite electronic dephasing times have to be considered on this time scale.

Optical dephasing studies, like line-shape analysis or the photon echo, can be used to analyze the initial response using dye molecules as probe for solvation dynamics, since optical dephasing depends on $M(t)$ as well [5]. Electronic dephasing in large molecules is usually discussed in terms of the coherence loss of the transition dipole moment of a two-level system [5–14]. Experimental data presented here will be analyzed adopting this scheme too. Clearly, large molecules are multilevel systems, if one considers the vibrational sublevels of the Franck-Condon active vibrations explicitly. Staying with the two-level model is possible by incorporating the vibrational contribution to the molecular response in the form of a generalized line-shape function. For dynamic spectroscopy the *multimode Brownian oscillator* (MBO) model has been used more widely in the context discussed here to project the multilevel wave packet dynamics into a two-level scheme [5,14,15]. As the wave-packet dynamics depends on excitation wavelength, the parameters of the MBO model should depend also on wavelength. Studying this relation between inherent electronic dephasing and the observed optical dephasing is the objective of our work. For comparison the time correlator model will be used in absorption line-shape analysis. This model considers the vibrational motion explicitly that can be derived from resonance Raman spectra.

Optical dephasing above the 0-0 transition was studied experimentally by Fujiwara *et al.* using incoherent photon echoes from cresyl fast violet in cellulose [15], in which solvation dynamics is slow even at room temperature. They concluded that the faster dephasing above the 0-0 transition was caused by a vibrational contribution, i.e., by increased excited state vibrational excess energy and corresponding density of states. In this paper, we report an experimental study of vibronic dephasing in which the laser is tuned across the whole absorption band including the long-wavelength absorption tail of a dye in solution. We will show in the following that the dephasing rate undergoes a minimum to the red of the 0-0 transition for the heptamethine dye studied here.

In our experiments, dephasing was not studied by photon echoes but by time-resolved *forced light scattering* (FLS), since this method is particularly suited to suppress the effect of the nonresonant susceptibility that becomes larger in the wings of the absorption band [16]. In FLS, a grating is induced by broadband pump lasers, which is probed by diffracting an additional narrow-band laser. The principles of this method have been described in a previous paper [13]. For comparison of the dephasing measured by FLS using incoherent broadband pulses with standard approaches, complimentary results are reported also for solutions of 1,1′,3,3,3′,3′-hexamethylindotricarbocyanine iodide (HITCI) in ethylene glycol, that have been studied also by femtosecond photon echoes [10–12,14].

The next section contains experimental details of the broadband dye laser sources, used in this study, and the experimental results obtained by FLS followed by their analysis. The discussion section gives a qualitative interpretation of the results.

TABLE I. Broadband dye laser characteristics.

Laser dye	Solvent	Concentration ($g\,l^{-1}$)	Pump (nm)	Laser emission Center (nm)	typical FWHM (nm)
Coumarin 120	Methanol	0.33	355	440	9
Coumarin 47	Methanol	0.3	355	461	8
Coumarin 102	Methanol	0.4	355	477	11
Coumarin 152a	Methanol	1.0	355	508	14
Coumarin 307 & Coumarin 153	Methanol	0.2 & 2.0	355	536	10
Coumarin 153	Methanol	4.0	355	546	16
Rhodamine 6G	Methanol	1.2	355	585	10
Rhodamine 6G	Methanol	0.4	532	571	5
DCM	Methanol	0.35	532	634	19
DCM	DMSO	0.4	532	667	17
Pyridin 1	Methanol	0.3	532	693	16
Styryl 8	DMSO	0.15	532	770	19

II. EXPERIMENT

A. Laser sources

Application of incoherent light techniques relies on properly constructed broadband dye lasers. High outcoupling from the laser resonator is mandatory to avoid spectral line narrowing and sweeping during nanosecond laser emission [17]. On the other hand, amplified spontaneous emission sources exhibit a poor transverse beam profile. As a compromise we used an uncoated glass plate as output coupler in our broadband dye lasers. The laser resonators had also plane end mirrors, but an intracavity lens was introduced to obtain effectively a semiconfocal resonator. The latter was necessary to minimize the notorious problem of spectral substructures in the laser spectrum. All broadband lasers were transversely pumped with the second or third harmonic of a *Q*-switched Nd:YAG laser resulting in a laser pulse duration of 3.5 ns. The laser wavelength was tuned by changing the laser dye, its solvent, and its concentration. Table I gives a summary of the dye lasers used in this work. The coumarin 120 laser was rebuilt several times to study the reproducibility. The center wavelength varied between 439.5 and 442 nm and the full width at half maximum (FWHM) was between 8.8 and 10.1 nm. The spectral laser emission was checked prior to each FLS experiment.

All broadband dye laser spectra were nicely Gaussian with the exception of the styryl 8 dye (Radiant Dyes Laser Acc.). This laser spectrum is plotted on the left hand side in Fig. 1 together with those from pyridine 1 and rhodamine 6G (logarithmic ordinate scale). To the right, the noncollinear autocorrelation is plotted, which was measured with a 200 μm thick BBO crystal. For non-transform-limited broadband lasers, this autocorrelation has a background that decays on the scale of the nanosecond pulse duration. This background was normalized to unity in Fig. 1.

The narrow-band probe laser was either the second harmonic of the Nd:YAG laser or a dye laser. The Nd:YAG laser had an intracavity etalon for linewidth narrowing and the narrow-band dye laser used a grazing incidence arrangement. So in both cases the linewidth was $\sim 0.1\ cm^{-1}$.

B. Sample absorption, fluorescence, and Raman spectra

We studied solutions of bis-(dimethylamino)heptamethinium chloride in ethanol at 10^{-3} mol/l. The extinction of the parent molecule is plotted in Fig. 2(a) (solid line). Far to the red higher dye concentration is needed to obtain a detectable FLS signal. Thus experiments were carried out also using the solvent trifluoroethanol, which allows a concentration of 9×10^{-3} mol/l without evidence of dye aggregation. The normalized absorption spectra are the same for both solvents. HITCI was studied at 7×10^{-5} mol/l in ethylene glycol [Fig. 2(a), dashed line].

A photoisomer (2-3-mono-cis-heptamethine) is produced upon optical excitation of the heptamethine dye [18–20]. We controlled the isomerization by recording *coherent anti-Stokes Raman scattering* (CARS) spectra. The pump laser was fixed at 585 nm and the Stokes laser was scanned. In our experiments, sample cuvettes (thickness 200–500 μm) with the dye solution were placed in the focus (diameter ~ 60 μm) of the objective used to overlap the laser beams of the spectroscopic measurement (either FLS or CARS). Figure 2(b) shows the CARS spectrum of the ethanolic heptamethine solution obtained without using a prepulse (solid squares). There are weak Raman lines at 1122 and 1191 cm^{-1}. It is well known that the photoisomer has two strong Raman lines in this frequency range. To isomerize the heptamethine dye, a prepulse (wavelength 480 nm) was applied from the opposite direction with respect to the spectroscopic pulses. The time delay τ_{PP} between prepulse and the spectroscopic pulses measured from peak to peak had a jitter of ± 2 ns. The intensity of the prepulse was chosen to completely isomerize all dye molecules, which occurred for about 50 μJ at 150 μm focal size. Dramatic changes in the CARS spectrum can be seen in Fig. 2(b); note that identical pump and Stokes laser intensity were applied for both spectra shown in Fig. 2(b). The solid line in Fig. 2(b) is a fit to the spectrum assuming Raman lines at $1072\ cm^{-1}$ and $1122\ cm^{-1}$. The characteristic C-C-N vibration of the photoisomer at $1072\ cm^{-1}$ appears immediately after photoexcitation and can be followed for several microseconds indicating a correspondingly high lifetime even in the room temperature experiments considered here. From the low CARS intensity at $1072\ cm^{-1}$ without applying a prepulse, a maximum isomerization below 2% is estimated as result of the action of the spectroscopic pulses themselves. Thus the contribution of the photoisomer is negligible in the FLS experiment without prepulse excitation. The absorption of the isomer is known to be shifted to the red and is plotted also in Fig. 2(a) as dotted line [18].

The fluorescence of heptamethine was measured in a dilute solution using single photon counting to minimize self-absorption. Excitation was performed with an argon ion laser at 514.6 nm. The fluorescence spectrum is discussed in Sec. III C 2 in connection with the results obtained by FLS.

Intensities and frequencies of the Raman lines are needed to deduce the amount of electronic dephasing induced broadening from absorption line-shape analysis. The strong fluorescence from the dye solution does not allow us to record

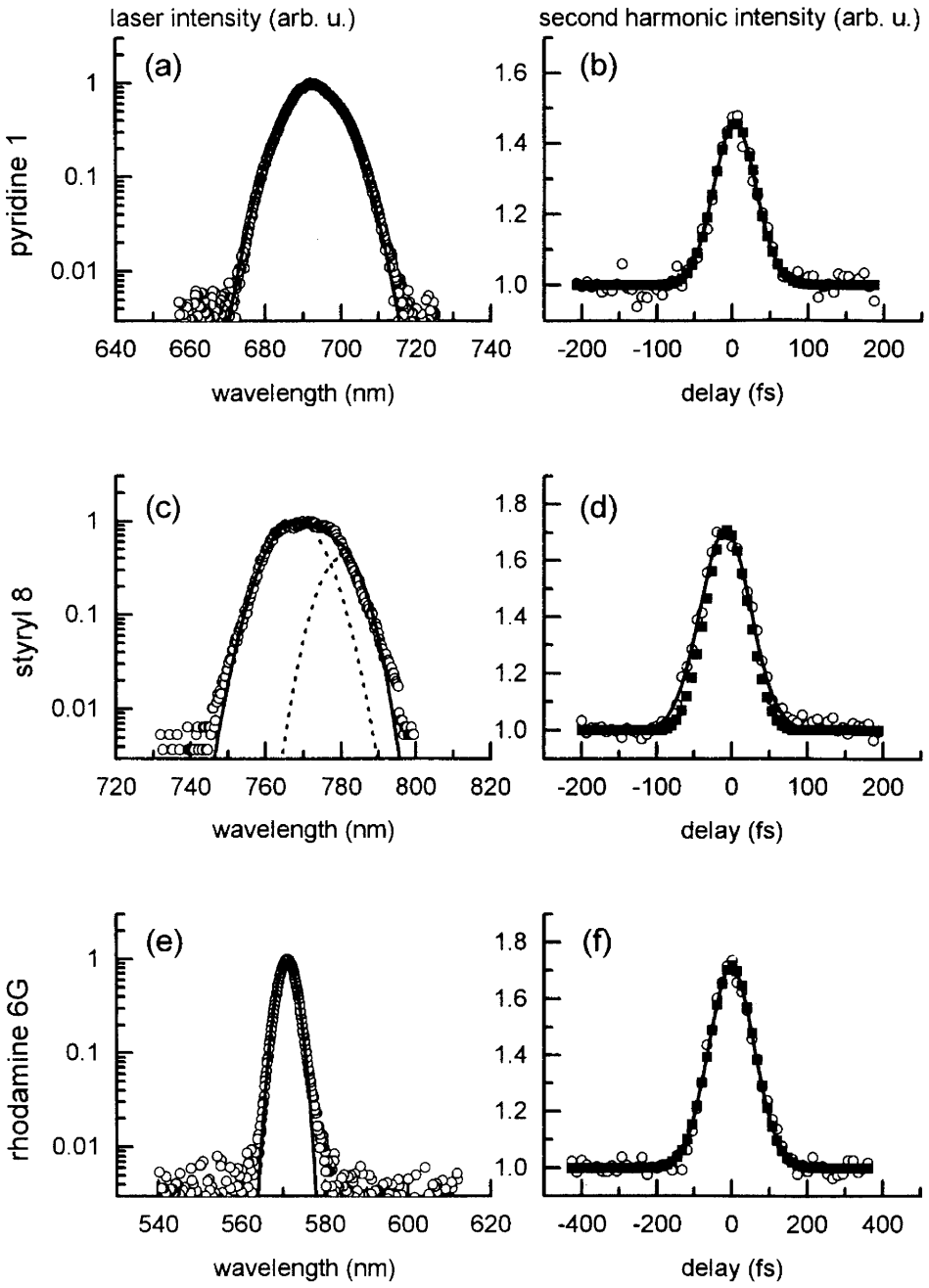

FIG. 1. Laser spectra and corresponding second-harmonic autocorrelation for three different broadband laser dyes; open circles: experiment; lines: Gaussian fits [double Gaussian in (c), dashed lines]; closed squares: calculated from laser spectrum by Wiener-Khintichine's theorem. There is a noticeable discrepancy to the solid line in (d).

resonance Raman spectra with excitation wavelength near the absorption maximum. The upper spectrum in Fig. 3 was recorded in methanolic solution exciting at 457.9 nm with an argon ion laser. The two strong Raman lines of methanol show up in the spectrum at 1034 and 1450 cm^{-1} and are marked by asterisks. Ethanol and trifluoroethanol have numerous Raman lines in the frequency range of Fig. 3 and were, therefore, not used as solvent. The fluorescence is considerably reduced in heptamethine crystals. The absorption maximum of the polycrystalline solid is shifted to 522 nm. The Raman spectrum shown as the lower trace in Fig. 3 was obtained with a Raman microscope in reflection geometry exciting at 488 nm with an argon ion laser. Both heptamethine spectra shown in Fig. 3 differ only by weak high-frequency modes. Such modes give negligible contributions in line-shape analysis (see below). The Raman spectrum of the crystal was used in absorption line-shape analysis, because it is not disturbed by solvent lines.

C. Forced light scattering

The two pump laser beams used for FLS were generated by beam splitting of broadband laser radiation in a Michelson interferometer. Their relative delay time will be denoted by τ in the following. Pump and narrow-band probe laser beams were overlapped in a phase matched folded box geometry. Details of the apparatus have been published elsewhere [13].

We checked the linewidth of the diffracted FLS signal at 440 nm pump laser wavelength and found no broadening within our experimental resolution of 1 cm^{-1} even for temporally overlapping pump and probe pulses. Diffraction is caused by slowly decaying gratings, such as thermal or population gratings, which do not lead to substantial spectral

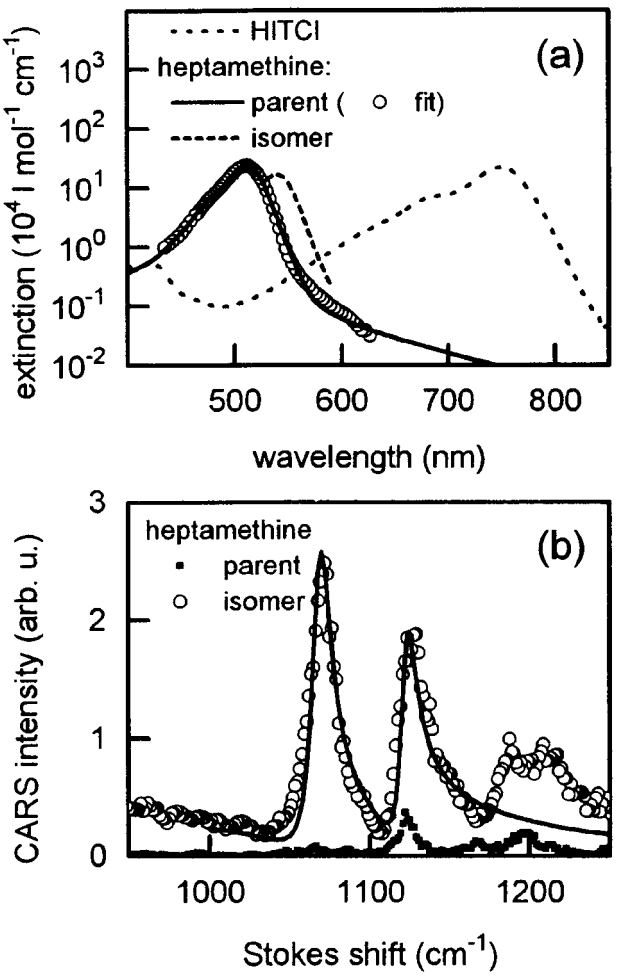

FIG. 2. Upper diagram: Extinction of dye solutions used in this study [symbols represent absorption line-shape analysis using Eqs. (7)–(10)]. Lower diagram: Scanning CARS spectra [solid squares: parent molecule; open circles: photoisomer generated by preexcitation at 480 nm; solid line: fit using two vibrational frequencies $\omega_j/(2\pi c)$, 1122 cm^{-1} and 1072 cm^{-1}; time delay $\tau_{pp}=198$ ns between excitation and spectroscopic pulses, narrowband pump laser at 585 nm, Stokes laser scanned 619–647 nm].

broadening of the diffracted beam. Thus no attempt was made routinely for spectral filtering of the signal (white detection limit).

Electronic dephasing was studied at different wavelength positions in the absorption band of the parent dye molecules as well as for the heptamethine photoisomer near its absorption peak. Figure 4 shows typical results for the measured FLS signal. To visualize qualitatively the broadening of the measured FLS signal as a function of delay time when increasing the pump laser wavelength, the abscissa was scaled to produce an equal width for the autocorrelation of the broadband laser, that would be expected from the laser spectrum by applying the Wiener-Khintchine theorem (see below) [13].

Table II summarizes the results obtained by FLS. The center wavelength of the applied broadband dye laser is given in each case and its emission bandwidth is expressed by the parameter W_D (see discussion section). The probe laser delay is the time interval between the two pump pulses

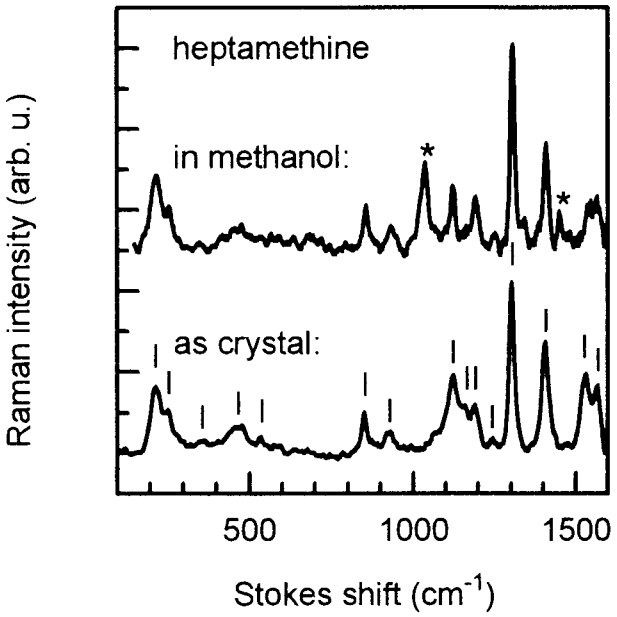

FIG. 3. Raman spectrum of heptamethine (slowly variant fluorescence background substracted). Upper spectrum: in methanol excited at 457.9 nm (asterisks indicate solvent lines). Lower spectrum: bulk crystals excited at full resonance at 488 nm (vertical bars indicate the Raman frequencies used in data analysis).

on the one side and the probe pulse on the other. W_E is the FWHM of the FLS signal as function of τ making a Gaussian fit to the experimental points. The quantity Δ_G characterizes the optical response of the dye solution for the respective pump laser wavelength (see below).

III. RESULTS

The most important result of this paper is the strong dependence of the dephasing rate Δ_G of heptamethine on the spectral position of excitation. Before we discuss this phenomenon in detail we will exclude artifacts which could contribute to this result. The knowledge of the field autocorrelation time of our broadband lasers is essential to carry out the deconvolution necessary to determine the molecular dephasing time. Up to now we calculated the correlation time of our broadband laser by the Wiener-Khintchine theorem only [13,16]. Here we present second-harmonic generation (SHG) measurements from which the autocorrelation time can be obtained on basis of experimental results (see subsection ''broadband laser second harmonic generation''). In a further step we proved the FLS method based on these nanosecond broadband lasers in comparing values provided by this method on the dye HITCI with results obtained by two pulse photon echoes using femtosecond pulses (see subsection ''HITCI''). Last, additional information was extracted from our resonance Raman spectra of heptamethine calculating the absorption line shape by the time correlator method (see subsection ''absorption line-shape analysis'').

A. Broadband laser second-harmonic generation

Second-order harmonic generation and forced light scattering are both second-order effects with respect to the broadband laser fields. However, since detection is per-

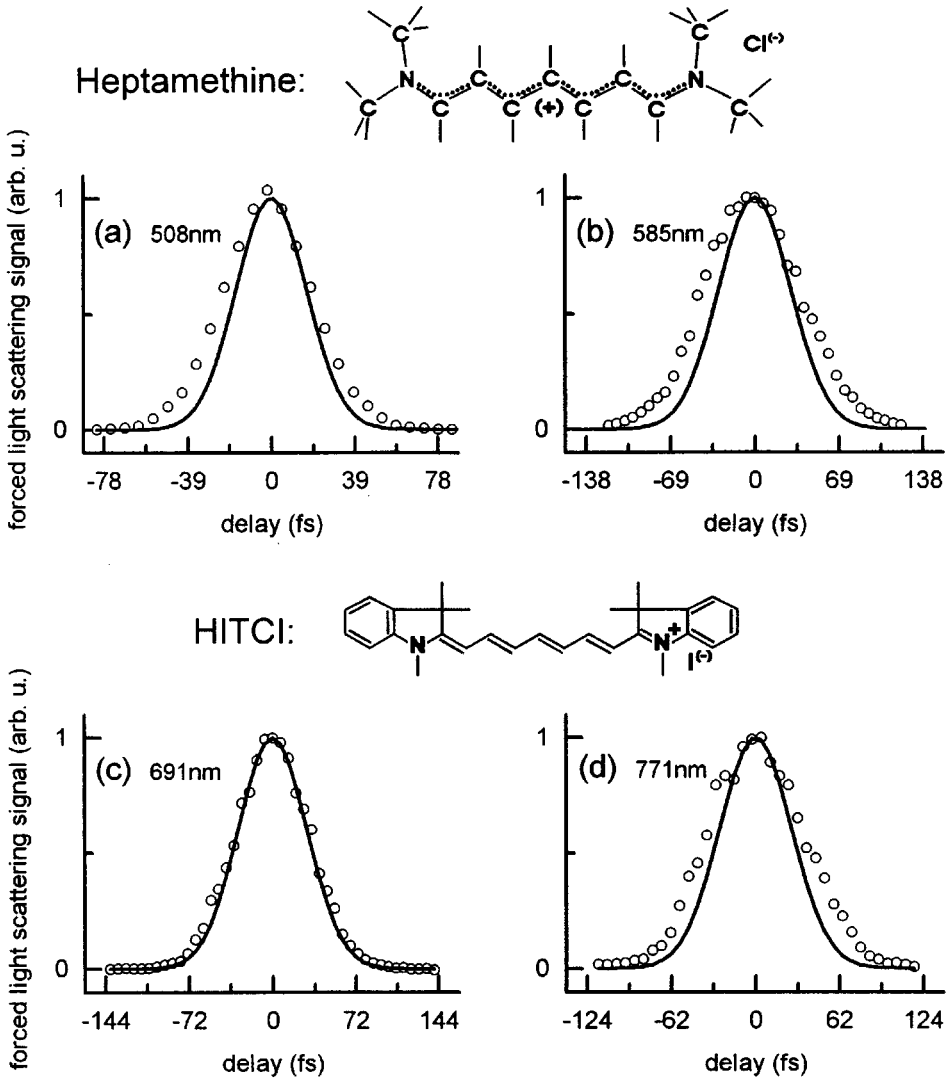

FIG. 4. FSL signal as function of relative pump delay time for two different dyes (chemical structures shown as header) above (a), (c) and below the 0-0 transition (b), (d). Open circles: FLS experiment; solid lines: autocorrelation functions calculated by Wiener-Khintchine theorem.

formed on intensity level, fourth-order correlation functions enter in both signals. The second-harmonic signal as function of delay is given by

$$I_{SHG}(\tau)=\langle R(t+\tau)R(t)R^*(t+\tau)R^*(t)\rangle, \tag{1}$$

where $R(t)$ is the randomly fluctuating part of the laser field obtained by separating the slowly varying pulse envelope. The brackets denote time average over the nanosecond pulse duration. The second-order correlation $D(\tau)$ can be calculated from the laser spectrum by the Wiener-Khintchine theorem:

$$D(\tau)=\langle R^*(t)R(t+\tau)\rangle \propto \int_0^\infty I_P(\omega)\ \exp\left[-i(\omega-\omega_P)\tau\right]d\omega, \tag{2}$$

where $I_P(\omega)$ is the spectral density of the broadband laser intensity [e.g., Figs. 1(a), (c), (e)]. The FWHM of the second-order correlation function as calculated from Eq. (2) is given in Table II as W_D. $R(t)$ is assumed to be a circular Gaussian complex random variable, i.e.,

$$\langle R(t)\rangle=\langle R(t_1)R(t_2)\rangle=0. \tag{3}$$

Hence the fourth-order correlation functions can be expressed by second-order correlation functions [21]. For the second harmonic one obtains

$$\begin{aligned} I_{SHG}(\tau)&=\langle R(t)R^*(t)\rangle\langle R(t+\tau)R^*(t+\tau)\rangle \\ &\quad+\langle R(t)R^*(t+\tau)\rangle\langle R(t+\tau)R^*(t)\rangle \\ &=1+|D(\tau)|^2 \end{aligned} \tag{4}$$

where the normalization $D(0)=1$ was applied.

A 2:1 contrast ratio is expected from Eq. (4). The experimentally observed contrast ratio is between 1.5:1 and 1.8:1 in Fig. 1. The lower experimental contrast ratio was explained by the multiple transverse mode emission of transversely pumped dye lasers [22]. Imperfect spatial overlap of the two pump pulses leads to SHG from different transverse modes which increases the base level.

The width of the coherence peak of the second harmonic should be identical to that calculated by Eq. (2). This is the case for the pyridine 1 laser and the rhodamine 6G laser in Fig. 1: the solid squares calculated by Eq. (2) lie on the lines that are fits to the second-harmonic signal. A 25% discrepancy is found for the styryl 8 laser [Fig. 1(d), see also Table II]. This, however, was the only dye laser used in this study

TABLE II. Results of forced light scattering experiments [λ: wavelength; W_D: calculated autocorrelation time of the broadband laser (SHG: result from second-harmonic generation experiment); W_E: measured width of the FLS signal; Δ_G: deduced dephasing rate].

Pump laser		Probe laser		FLS	
λ (nm)	W_D (fs)	λ (nm)	delay (ns)	W_E (fs)	Δ_G (THz)
		HITCI			
691	72	532	8	75	81
771	62	532	12	83.6	30
	(SHG 79)				(SHG 61)
		All-*trans*-heptamethine			
440	45.5	532	8	47.6	120
442	45.4	532	8	46.5	166
441	39.8	730	0	43.2	99
461	53.6	532	8	57.5	80
508	38.7	550	0	49	55
536	57.6	572	0	68.9	44
546	37.6	465	0	38.9	-
		730	0	48.1	55
585	69.3	660	0	94.2	26
571	120	730	0	132	30
	150	560	12	166	23
634	43.5	730	0	57.6	44
667	51.0	730	0	54.9	82
		2,3-mono-*cis*-heptamethine			
536	57.6	572	0	63	63
585	69.3	660	0	85	33

that was not emitting a Gaussian laser spectrum. The spectrum displayed in Fig. 1(c) could be explained by a mixture of laser emission and superluminescence, that broadens the spectrum on the long wavelength side. Figure 1(c) shows a double Gaussain fit to the experimental spectrum with one subline centered at 768 nm having a width that corresponds to correlation function measured by SHG. Superluminescence has a much higher beam divergence and therefore does not contribute significantly to the second harmonic because of its low focal intensity. So the measured width of the second-harmonic coherence spike can be interpreted as true laser correlation width.

B. HITCI

In the theory applied here for data analysis, the probe laser field invention is assumed to be after both pump field actions [13]. This is definitely justified for the FLS experiments with HITCI since pump and probe pulses were separated on a nanosecond time scale (for zero delay see below). The optical dephasing of HITCI in ethylene glycol was measured by short pulse photon echoes [10,11,14]. The line broadening functions $g(t)$ used to fit those experiments are plotted in Fig. 5. They are in good approximation quadratic functions, so that response functions of the form

$$\exp[-g(t)] = \exp(-\Delta_G^2 t^2/2) \tag{5}$$

will be used in the following to fit the FLS signal, where Δ_G is regarded as a fit parameter.

The delay time dependence of the FLS signal intensity can be calculated from [13]:

$$I_{\mathrm{FLS}}(\tau) \propto \mathrm{const} + \left| \int_{-\infty}^{\infty} D(t-\tau) \ \exp[-g(|t|)]dt \right|^2, \tag{6}$$

where the correlation function $D(t)$ can be taken from Eq. (2) or from the coherence spike measured by second-harmonic generation. This leads to an ambiguity only for the experiment with the styryl 8 laser. The solid line in Fig. 5 was obtained with 20 fs pulses matching the dye's fluorescence maximum at 770 nm [11]. Analyzing the results of Fig. 4(d) with the experimental correlation width in Fig. 1(d) gives $\Delta_G = 61$ THz, which fits the photon echo result of Ref.

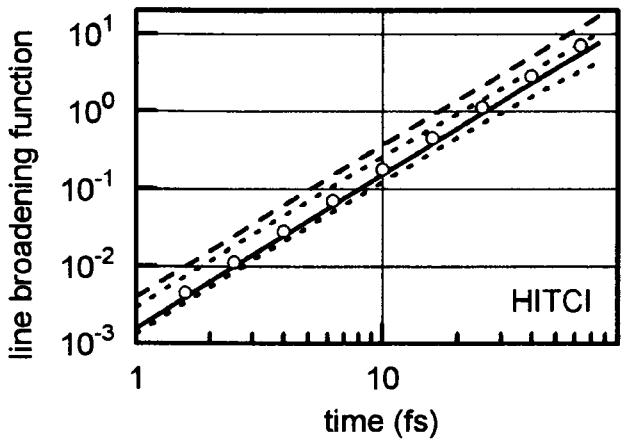

FIG. 5. Line-broadening functions describing the optical dephasing of HITCI in ethylene glycol; open circles: FLS experiment; lines: femtosecond photon echo ([10]: dotted lines; [11]: solid line; [14]: dashed line).

[11] within 10% (open circles). Calculating $D(t)$ from Fig. 1(c) (non-Gaussian intensity spectrum) would have given the incorrect value $\Delta_G = 30$ THz. This shows that, providing correct deconvolution of Eq. (6), FLS can be used to determine dephasing rates, making it an alternative method to the two pulse photon echo. FLS based on excitation with broadband nanosecond laser pulses has a very high efficiency, but a limited dynamic range of measurement. Due to the high efficiency FLS enables one to measure dephasing rates in a broad spectral region, far broader than the absorption band of the chromophore under investigation. Therefore dephasing rates far off the resonance can be performed. Due to the limited dynamic range information of the early contribution to the dephasing rate can only be obtained (approximation by a Gaussian function). Whereas for FLS (as well as for two-pulse photon echo) it is not possible to separate contributions of fast and slow processes to the dephasing rate, as can be done by fifth-order three-pulse photon echoes [23] or phase-locked heterodyne photon echo techniques [24], the wide wavelength range of possible excitation can provide additional insight into the role of vibrations for ultrafast dephasing.

For HITCI excitation at a second wavelength position at 691 nm was carried out. For the applied broadband laser with pyridine as active dye the Wiener-Khintchine theorem and second-harmonic coherence spike give identical correlation widths. At 691 nm, $\Delta_G = 81$ THz is obtained. This value is noticeably higher than at 771 nm.

C. Heptamethine

1. Temporally overlapping pump and probe pulses

Most of the FLS experiments with the heptamethine dye were carried out with temporally overlapping pump and probe laser pulses, because this gives the highest signal level. In this case the spectral position of the probe laser is relevant (see Table II for a pump wavelength of 546 nm). Coherent coupling between pump and probe laser pulses is possible, i.e., diagrams with field action of the probing pulse before action of the pump pulses have to be considered. These contributions have been analyzed theoretically by Yang *et al.* on the basis of Lorentzian spectral densities [25]. They are important, if the absorption at probe laser wavelength is not small compared to the absorption at the pump laser wavelength, provided that the spectral width of the laser is small compared to the width of the absorption line. In addition, pump probe coupling mediated by a high-frequency Raman resonance has too low efficiency for heptamethine, as the origin shifts are small for high frequencies, as shown in Sec. III C 3.

We checked these theoretical considerations for a pump laser wavelength of 546 nm using two different probe laser wavelength values: 465 nm and 730 nm (Table II). The extinction of the heptamethine dye is 2.5 times higher at 465 nm than at 546 nm (pump laser). So for these special conditions the additional contributions might even dominate the signal. The negligible difference between the observed width $W_E = 38.9$ fs and the autocorrelation width $W_D = 37.6$ fs does not therefore imply a nearly instantaneous optical dephasing at 546 nm. At 730 nm the absorption for the probe beam is more than 100 times less, allowing us to use Eq. (5)

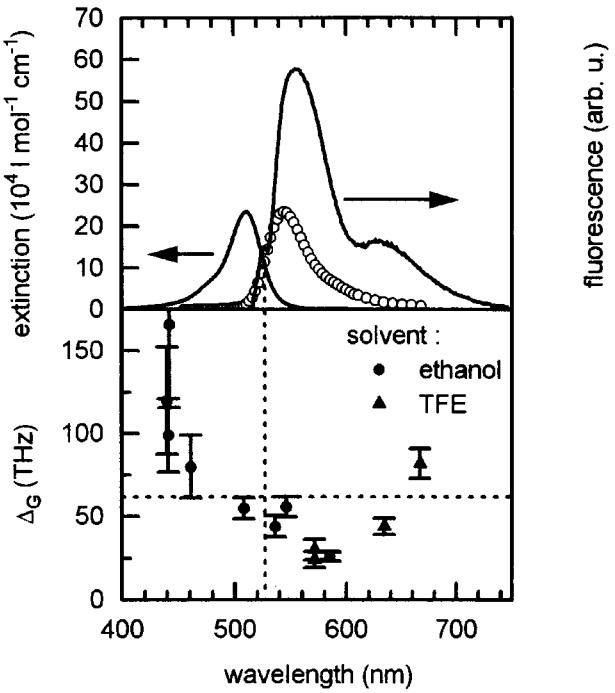

FIG. 6. Comparison of wavelength dependent optical dephasing of heptamethine solutions (lower diagram, TFE: solvent trifluoroethanol) with linear absorption and fluorescence (upper diagram). The minimum dephasing rate is observed to the red of the fluorescence maximum. Dotted lines: vertical: wavelength position of 0-0 transition; horizontal: dephasing rate calculated from absorption line shape ignoring vibrational contribution. Open circles: mirror image of the absorption spectrum.

for data analysis, giving $\Delta_G = 55$ THz (Table II).

2. Wavelength dependence of optical dephasing

The quantity Δ_G derived from the experiment is plotted as function of pump laser wavelength at the bottom of Fig. 6. The spread of the data points at ~ 440 nm can be explained by an uncertainty of 0.5% for W_E and W_D. The error bars in Fig. 6 are calculated assuming twice this uncertainty. The optical dephasing rate shows a pronounced minimum at about 580 nm. This minimum lies to the red of the spectral position of the fluorescence maximum.

In the upper part of Fig. 6 a fluorescence spectrum is shown obtained exciting the solution of heptamethine at 514.6 nm (solid line). Even qualitatively the fluorescence is not the mirror image of the absorption spectrum that is indicated also in Fig. 6. This is not surprising, since the quantum yield for isomerization is rather high (about 0.7 [18]), so that there are dominant contributions from other molecular configurations. Time resolved CARS experiments and quantum chemical calculations have shown that the excited state of heptamethine has a double well potential [26]. The *trans-cis* isomerization proceeds through an intermediate state twisted by 90° out of the molecular plane. All of these states can contribute to the fluorescence. The fluorescence peak at 555 nm is shifted by 1550 cm^{-1} with respect to the absorption maxima of the parent molecule (511 nm). The 0-0 transition lies exactly in the middle (on the frequency axis) between absorption and fluorescence maximum provided they are

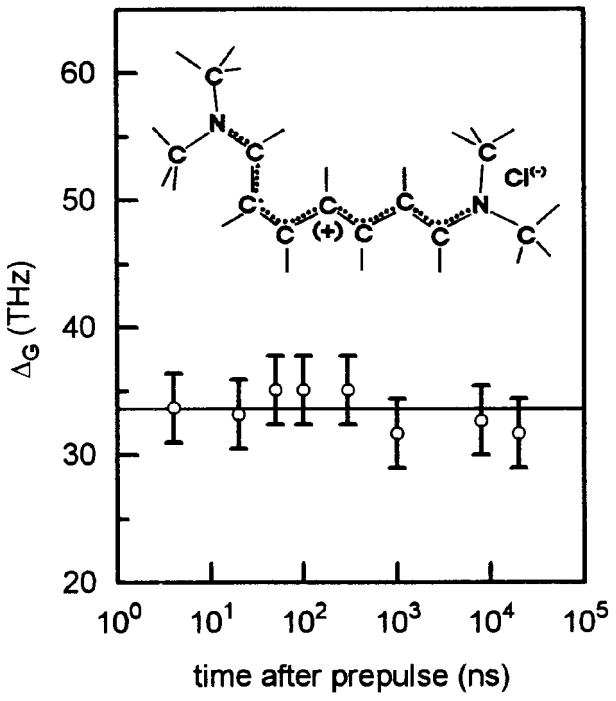

FIG. 7. Optical dephasing of the heptamethine solution observed at 585 nm for different times τ_{pp} between prepulse and FLS experiment (chemical structure of the investigated 2,3-mono-*cis*-heptamethine shown as inset).

mirror images. As the latter is not the case (Fig. 6), the position can only be estimated to be near 532 nm. Previous absorption line-shape analysis have put the spectral position of the 0-0 transition in the range from 518 to 523 nm [27]. However, only raw fits were made assuming Lorentzian spectral densities. An advanced analysis will be given below that gives an improved fit to details of the absorption line shape.

Comparing the dephasing measured for the isomer with that found without prepulse excitation (parent molecule) shows slightly higher values for the isomer for the same wavelength (Table II). The FLS experiment was repeated for different times intervals between prepulse and the FLS pulses from partial pulse overlap up to several microseconds. The deduced dephasing rate remains constant within experimental uncertainty (Fig. 7). This indicates that photochemical dynamics plays no role on a nanosecond time scale, and that the isomer behaves like an ordinary dye molecule immediately after photoproduction. The slightly higher dephasing rate for the isomer was expected from the redshift of the absorption maximum compared to the parent molecule.

3. Absorption line-shape analysis

Absorption line-shape analysis is based here on the time correlator model that was introduced around 1980 [28]. In this model the line-broadening function is a sum of a pure electronic contribution and the vibrational contribution [5,29,30]:

TABLE III. Raman active modes and their squared origin shift as derived from resonance Raman intensities for heptamethine crystals (excitation 488 nm).

Mode frequency (cm^{-1})	Integrated Raman intensity (arb. units)	Squared origin shift (arb. units)
216	45	1.00
255	57	0.95
357	14	0.10
465	43	0.16
537	5	0.01
852	17	0.01
927	22	0.01
1122	75	0.03
1164	12	<0.01
1191	15	<0.01
1239	16	<0.01
1303	80	0.03
1406	64	0.03
1529	100	0.05
1569	41	0.02

$$g_A(t)=g_E(t)-Z\sum_{j=1}^{N} z_j^2[(\overline{n_j}+1)\ \exp\ (-i\omega_j t) + \overline{n_j}\ \exp\ (i\omega_j t)]. \tag{7}$$

The sum in Eq. (7) runs over the most prominent Raman active vibrational modes (frequency ω_j, squared origin shift z_j^2, thermal population number $\overline{n_j}$), Z being an overall weighting factor for the vibrational contribution resulting from absolute values of the Franck-Condon factors. Raman frequencies and squared origin shifts were deduced from the Raman spectrum depicted in Fig. 3 following the procedure outlined in Ref. [29]. The results are given in Table III. As the z_j^2 were normalized so that $z_j^2=1$ for the $216\,cm^{-1}$ mode, Z is the absolute value of the squared origin shift of this mode.

Different forms of the electronic part are assumed in literature for absorption line-shape analysis. In Ref. [27] a simple homogeneously broadened electronic transition was assumed, i.e., $g_E(t)=\Gamma t$. It is well known that such an approximation cannot fit the wings of the absorption band as the experimental absorption drops much more rapidly on the long wavelength side. Nice fits were obtained for a different dye by using the Bloch model,

$$g_E(t)=\Gamma t+\Delta^2 t^2/2, \tag{8}$$

where Γ was interpreted as homogeneous broadening and Δ can either represent an inhomogeneous broadening or the cumulative effect of low frequency bath modes on dephasing [29], We will use this approach too. Alternatively, the Kubo model can be used [10–14], where

$$g_E(t)=\Delta_K^2/\Lambda_K^2[\exp\ (-\Lambda_K t)+\Lambda_K t-1]. \tag{9}$$

Here Λ_K is the inverse of the bath correlation time and Δ_K is the modulation strength.

Linewidth broadening caused by finite excited state lifetime of the order of 30 ps is negligible in absorption spectra of dye molecules in solution, so that the absorption is given by

$$A(\omega) \propto \mathrm{Re} \int_0^\infty dt \, \exp\,[i(\omega-\omega_{00})t - g_A(t)], \qquad (10)$$

where ω_{00} is the 0-0 transition frequency. The simulation used $Z=1.15$, $\Gamma=15$ THz, and $\Delta=53$ THz for the Bloch model. The absorption is well reproduced by this parameter set for the whole wavelength range studied by forced light scattering (Fig. 2). The circles in Fig. 6 were calculated by reflecting the absorption curve at the position of the 0-0 transition, that was calculated to be at $2\pi c/\omega_{00}=527$ nm. This wavelength position is indicated in Fig. 6 as a vertical dotted line. The magnitude of the calculated curve was normalized with respect to the experimental fluorescence in a way that the integrated fluorescence corresponds to the quantum yield of 30% for recovering the all-*trans* configuration after an optical excitation cycle. Noteworthy, equivalently nice fits to the absorption are obtained using the Kubo model with $\Lambda_K=6.5$ THz and $\Delta_K=62$ THz.

IV. DISCUSSION

A. Magnitude of the dephasing rate

Line-shape analysis of stationary absorption spectra assumes a single electronic sublevel that is dressed by coupling to vibrational modes that are seen in resonance Raman spectra. A broadening by other interactions is not resolved. Forced light scattering offers an additional insight as interactions between sublevels not covered by the laser spectrum do not contribute to the measured dephasing as long as they are slow compared to the time resolution indicated by the actually measured width W_E; i.e., the additional information comes from the ability to perform a kind of transient hole burning. The dephasing rate constant Δ_G has the meaning of the linewidth of the transient hole that is assumed to have Gaussian shape. A slow interaction is responsible for the relaxation to the whole absorption linewidth seen in linear spectroscopy. This process can be called spectral cross relaxation.

The line-broadening function as given by Eq. (7) is complex. In order to facilitate a comparison with the model of Eq. (5), we insert the line-broadening function (7) in Eq. (6) assuming a Gaussian autocorrelation function $D(\tau)$ of the laser pulse. The resulting $I_{\mathrm{FLS}}(\tau)$ is also Gaussian down to the percentage level, provided that the width of $D(\tau)$ is larger than 20 fs, so that the vibrational motions do not become resolved. The deduced Δ_G resulting from deconvoluting of this calculated $I_{\mathrm{FLS}}(\tau)$ is equal to 140 THz, which corresponds to the overall absorption linewidth. So this value can be compared with the measured FLS data plotted in Fig. 6. All measured values of Δ_G are less to or equal than 140 THz and in addition they show a wavelength dependence, discussed below.

The model used to derive Eq. (7) makes three simplifying assumptions: First, the Condon approximation ignores any dependence of the electronic transition moment on nuclear coordinates. Second, equal vibrational frequencies and normal coordinates are assumed for all electronic states. Third, only one excited electronic state is assumed. Molecular-orbital calculations strongly suggest that the third assumption is correct for the heptamethine absorption at 511 nm [31]. The second assumption cannot be fully correct because photoisomerization takes place. This could allow one to minimize the vibrational contribution. If the vibrational contribution in $g_A(t)$ is neglected, then $\Delta_G=65$ THz rather than 140 THz is calculated (Fig. 6, horizontal dotted line). However, the lowest experimental Δ_G are less than half this value. This demonstrates that either the Condon approximation is violated or the vibrational contribution to the total dephasing in the 140 THz width is higher than calculated by Eq. (7). A considerable contribution of photoisomerization to optical dephasing was already discussed for bacteriorhodopsin [32]. These calculations indicate that indeed the vibrational contribution to dephasing is underestimated in general by Eq. (7) in the case of complicated excited state potentials. So the discrepancy between the calculated 65 THz and the minimum observed value of (25 ± 10) THz does not indicate a violation of the Condon approximation.

In general, observing a smaller dephasing rate than given by the overall absorption linewidth is indicative of inhomogeneous broadening. In room-temperature liquids this inhomogeneous broadening disappears typically on a time scale up to 1 ps, which is called spectral cross relaxation time [9]. For longer time scales the absorption line appears to be essentially homogeneously broadened. The spectral cross relaxation is explained by nuclear motions in the solvent molecules. In the case of heptamethine, however, the reason for observing small dephasing rates around 580 nm is most likely related to complicated intramolecular nuclear motions. So the transition to the homogeneously broadened absorption line seen by linear spectroscopy is a spectral cross relaxation in a broader sense, since it arises from an intramolecular interaction. Of course, as in other two-photon experiments, no decisions can be made between contributions of different fast and slow dephasing processes to Δ_G by forced light scattering, so that the dynamic of this spectral cross relaxation cannot be resolved.

B. Wavelength dependence of the dephasing rate

All dyes studied in this work have in common that the optical dephasing relevant to FLS experiments becomes faster when the pump laser is tuned to the blue side of the 0-0 transition. Such an accelerated dephasing in the blue side of the absorption band was reported earlier for incoherent photon echoes [15,33]. These observations were explained by considering the vibrational contribution to dephasing of the electronic transition. Exciting to the blue of the 0-0 transition, as in our experiment at 691 nm for HITCI, prepares highly nonstationary wave packets that move out of the Franck-Condon region very quickly [33]. This process reduces the coherent polarization detected by the second delayed pulse. Thus the optical dephasing is faster to the blue side of the 0-0 transition. This basic effect is a result of probing at different wavelength positions in a multilevel system.

Wave-packet dynamics is usually analyzed assuming parabolic potentials [32]. Stationary excited state wave packets are expected for exciting to the minimum of the excited state potential, which coincides with the frequency position of the relaxed fluorescence maximum. This is correct even if there are different vibrational frequencies or normal modes in the excited state. However, ground state wave-packet motion can contribute to dephasing as well. Ground state wave-packet motion is smallest for excitation at the absorption maximum. So the minimum vibronic dephasing is expected to be exciting at or near the 0-0 transition. This is not the case for the heptamethine dye concerning the calculated position of the 0-0 transition, as minimum dephasing is observed at 570–580 nm, a position which is shifted even to the red of the fluorescence maximum.

Most relevant in discussing this discrepancy is to note that the heptamethine dye can have a variety of isomeric structures, the all-*trans* configuration (shown in Fig. 4) being the most stable isomer in the ground state. Thermal excitation could potentially generate other isomers. The CARS experiment can only pose an upper limit of 2% for the isomer concentration [Fig. 2(b)]. The fit to the absorption line shape is nice even up to 620 nm, so that there is no indication of other isomers being present prior to optical excitation. Corresponding to the high isomerization efficiency of 0.7 upon photoexcitation near the absorption maximum, the most stable configuration in the excited state is the 2,3-mono-*cis* isomer (structure shown in Fig. 7). Thus the excited state potential energy surface cannot be parabolic with the same curvature as in the ground state. This argument is supported by the complicated fluorescence spectrum. The minimum of the dephasing rate observed far to the red of the 0-0 transition could therefore be related to the complicated potential energy surface, which might have minimum vibrational dynamics contribution at $\sim$580 nm. Correspondingly, the increased values of Δ_G at even larger wavelengths could also be interpreted as result of a growing contribution of excited vibrations.

V. CONCLUSIONS

The feasibility of using forced light scattering to measure electronic dephasing was demonstrated by comparison with two pulse femtosecond photon echoes from HITCI, yielding equivalent results. Electronic dephasing of *all-trans*-bis-(dimethylamino)heptamethinium and its photoproduced, metastable isomer was studied experimentally in detail by excitation in a very broad spectral region from 440 nm up to 667 nm making use of the high efficiency of FLS. The speed of optical dephasing shows a pronounced minimum to the red of the (calculated) 0-0 transition. The broadening parameter deduced by deconvolution is larger for the isomer than for the parent molecule, which can presumably be attributed to the redshifted absorption band of the isomer. A qualitative physical explanation for the wavelength dependence of the dephasing rate is given considering different molecular configurations in the excited state and different contributions from vibronic states. Excitation at higher vibronic states prepares wave packets moving faster out of the Franck-Condon region the more vibronic levels are involved, reducing thereby the coherent polarization detected by the second delayed pulse. A quantitative description of optical dephasing requires further work. Comparison with absorption lineshape analysis indicates a considerable spectral cross relaxation for the heptamethine dye.

ACKNOWLEDGMENTS

This work was supported by the Deutsche Forschungsgemeinschaft. We thank R. Goleschny for technical support, and Dr. M. Pfeiffer and Professor T. Elsässer for stimulating discussions. We are very grateful to Dr. L. Dähne, Free University Berlin, for providing the heptamethine dye.

[1] R. J. Jimenez, G. R. Fleming, P. V. Kumar, and M. Maroncelli, Nature **369**, 471 (1994).
[2] M. Maroncelli, J. Mol. Liq. **57**, 1 (1993).
[3] T. Fonseca and B. M. Ladanyi, J. Phys. Chem. **95**, 2116 (1991).
[4] L. E. Fried, N. Bernstein, and S. Mukamel, Phys. Rev. Lett. **68**, 1842 (1992).
[5] S. Mukamel, Annu. Rev. Phys. Chem. **41**, 647 (1990).
[6] P. C. Becker, H. L. Fragnito, J.-Y. Bigot, C. H. Brito Cruz, R. L. Fork, and C. V. Shank, Phys. Rev. Lett. **63**, 505 (1989).
[7] J.-Y. Bigot, M. T. Portella, R. W. Schoenlein, C. J. Bardeen, A. Migus, and C. V. Shank, Phys. Rev. Lett. **66**, 1138 (1991).
[8] E. T. J. Nibbering, D. A. Wiersma, and K. Duppen, Phys. Rev. Lett. **66**, 2464 (1991); **68**, 514 (1992).
[9] T. Joo and A. C. Albrecht, Chem. Phys. **176**, 233 (1993).
[10] M. S. Pshenichnikov, K. Duppen, and D. A. Wiersma, Phys. Rev. Lett. **74**, 674 (1995).
[11] P. Vöhringer, D. C. Arnett, R. A. Westervelt, M. J. Feldstein, and N. F. Scherer, J. Chem. Phys. **102**, 4027 (1995).
[12] P. Vöhringer, D. C. Arnett, T.-S. Yang, and N. F. Scherer, Chem. Phys. Lett. **237**, 387 (1995).
[13] A. Kummrow, A. Lau, and S. Woggon, Phys. Rev. A **50**, 4264 (1994).
[14] W. P. deBoeij, M. S. Pshenichnikov, K. Duppen, and D. A. Wiersma, Chem. Phys. Lett. **224**, 243 (1994).
[15] M. Fujiwara, R. Kuroda, and H. Nakatsuka, J. Opt. Soc. Am. B **2**, 1634 (1985).
[16] A. Kummrow, Chem. Phys. Lett. **236**, 362 (1995).
[17] Y. H. Meyer, O. Benoist D'Azy, M. M. Martin, and E. Bréhéret, Opt. Commun. **60**, 64 (1986).
[18] S. Rentsch, thesis, Friedrich-Schiller-Universitat, 1982 (unpublished).
[19] W. Werncke, A. Lau, M. Pfeiffer, H.-J. Weigmann, W. Freyer, Jong Tscholl Tschö, and Man Bok Kim, Chem. Phys. **118**, 133 (1987).
[20] A. Lau, W. Werncke, M. Pfeiffer, H.-J. Weigmann, and Kim Man Book, J. Raman Spectrosc. **19**, 517 (1987).
[21] J. W. Goodman, *Statistical Optics* (Wiley, New York, 1985).
[22] T. Hattori, A. Terasaki, and T. Kobayashi, Phys. Rev. A **35**, 715 (1987).

[23] T. Joo, Y. Jia, and G. R. Fleming, J. Chem. Phys. **102**, 4063 (1995).
[24] M. S. Pshenichnikov, W. P. de Boeij, and D. A. Wiersma, Phys. Rev. Lett. **76**, 4701 (1996).
[25] T.-S. Yang, R. Zhangh, and A. B. Myers, J. Chem. Phys. **100**, 8573 (1994).
[26] A. Lau, W. Werncke, M. Pfeiffer, H.-J. Weigmann, and Kim Man Bok, J. Raman Spectrosc. **19**, 517 (1988).
[27] P. P. Kircheva, M. Pfeiffer, A. Lau, and W. Werncke, J. Raman Spectrosc. **20**, 183 (1989).
[28] J. B. Page and D. L. Tonks, J. Chem. Phys. **75**, 5694 (1981); S.-Y. Lee and E. J. Heller, *ibid.* **71**, 4777 (1979).
[29] K. Lenz, M. Pfeiffer, A. Lau, and T. Elsaesser, Chem. Phys. Lett. **229**, 340 (1994).
[30] M. K. Lawless and R. A. Mathies, J. Chem. Phys. **96**, 8037 (1992).
[31] M. Pfeiffer, W. Werncke, A. Lau, and W. Freyer, in *Electronic Properties of Polymers*, edited by H. Kuzmany, M. Mering, and S. Roth (Springer, Berlin, 1992), p. 150.
[32] W. T. Pollard, S. Y. Lee, and R. A. Mathies, J. Chem. Phys. **92**, 4012 (1990).
[33] Y. Zhang, F. Moshary, and S. R. Hartmann, Laser Phys. **5**, 676 (1995).